chemosensors

Communication

A Theoretical Examination of Various Complexes of a Proposed Novel Chemosensor Material—Graphene/SiC

Dobromir A. Kalchevski [1], Stefan Kolev [1], Dimitar Dimov [1], Dimitar Trifonov [1], Ivalina Avramova [2,*], Pavlina Ivanova [1] and Teodor Milenov [1]

[1] "Acad. E. Djakov" Institute of Electronics, Bulgarian Academy of Science, 72 Tzarigradsko Chaussee Blvd., 1784 Sofia, Bulgaria; skkolev@ie.bas.bg (S.K.); dadimov@ie.bas.bg (D.D.); dtrifonov@ie.bas.bg (D.T.); ivanovap@ie.bas.bg (P.I.); tmilenov@ie.bas.bg (T.M.)

[2] Institute of General and Inorganic Chemistry, Bulgarian Academy of Sciences, Acad. G. Bonchev Str., bl. 11, 1113 Sofia, Bulgaria

* Correspondence: iva@svr.igic.bas.bg

Abstract: The potential of semiconducting, corrugated graphene, grown on silicon carbide, as an active element in chemosensors is studied in the present work. For this purpose, the adsorption of benzene, diazepam and 2,3,7,8-tetrachlorodibenzo-*p*-dioxin (TCDD) on the material's surface was modeled. According to the graphene sheet bending and adsorbate–adsorbent distances, the heterostructure favors the ligands in the order of diazepam < benzene < TCDD. The apparent ambiguity in the results for diazepam is easy to explain. The abundance of lone pairs and π-electrons compensates for the low-symmetry, non-planar, far from optimal (adsorption-wise) geometry. The maximum band gap change in the heterostructure, caused by adsorption, is 0.02 eV. Intermolecular binding does not alter the HOMO–LUMO difference in benzene and TCDD by more than 0.01 eV. The completely planar molecules are not expected to undergo significant geometrical changes; hence, the alteration in their frontier orbitals is also minimal. The adsorption of diazepam, however, causes significant changes in the projected density of states of both structures in the complex. In conclusion, corrugated graphene is applicable as an active material in selective chemosensors for non-planar aromatic molecules.

Keywords: ab initio simulations; graphene; SiC; chemodetection

Citation: Kalchevski, D.A.; Kolev, S.; Dimov, D.; Trifonov, D.; Avramova, I.; Ivanova, P.; Milenov, T. A Theoretical Examination of Various Complexes of a Proposed Novel Chemosensor Material—Graphene/SiC. *Chemosensors* **2024**, *12*, 239. https://doi.org/10.3390/chemosensors12110239

Received: 11 October 2024
Revised: 12 November 2024
Accepted: 14 November 2024
Published: 17 November 2024

1. Introduction

As is well known, there are several methods for the reproducible synthesis of graphene for applications in electronics: chemical vapor deposition (CVD) techniques and so-called epitaxial growth on SiC. The former method is usually associated with the deposition of graphene on a catalytically active metal foil (usually Cu or Ni) in processes involving the thermally stimulated decomposition of a hydrocarbon precursor (usually methane) [1–4]. The resulting graphene films have high quality but are not convenient for direct use in electronics because they must be transferred onto other substrates.

The latter method, usually defined as the termination of either the (111)Si or (111)C faces of SiC substrates/films, was actually described before CVD techniques [5]. In this method, SiC substrates with their $(111)_{Si}$ or $(111)_{C}$ faces are annealed at very high temperatures (usually up to 1400 °C) and under a high vacuum, which, after the sublimation of the Si atoms from the surface and the rearrangement of the atoms, results in the completely controlled and reproducible formation of single- or bi-layer graphene on SiC. Later, it was established that the first graphene layer, the so-called buffer layer (BL), is periodically corrugated [6]. This corrugation is almost unequivocally associated with the covalent bonding of some C atoms from the graphene sheet with Si atoms from the surface of the SiC, i.e., with a change in the hybridization of C atoms in certain atomic positions of BL from sp^2 to sp^3. Later, it was established that, during graphene synthesis on the silicon side of multilayer

polytypes 4H-SiC or 6H-SiC, the cases most often used in practice, the resulting periodic structure is with an elementary cell of $6\sqrt{3} \times 6\sqrt{3}$R30, denoted simply as 6R3. However, it should also be noted that a modulation of the type 6×6 and $\sqrt{3} \times \sqrt{3}$R30, denoted as R3, was observed in some cases [7].

Subsequent theoretical studies (see [8,9]) showed that, due to the change in the hybridization of the carbon atoms of BL graphene, a band gap is induced in it, and its width is related to the corrugation period. In parallel, our theoretical studies have shown that the adsorption of different molecules on an ideal graphene sheet induces different changes in the conductivity of the graphene states, i.e., the graphene sheet can be used to detect different organic molecules [10].

As discovered in our previous publication, due to covalent Si–C bonding in the heterostructure, the graphene sheet is corrugated and possesses a band gap [8]. In the present work, we theoretically evaluate the chemosensory properties of the adsorbent material BL graphene (G) on silicon carbide (SiC) by studying the complexation of three adsorbates (A): benzene (PhH), diazepam (D) and 2,3,7,8,-tetrachlorodibenzo-P-dioxin (TCDD). Diazepam is a well-known drug substance, while PhH and TCDD are high-risk carcinogenic chemicals [11,12].

2. Materials and Methods

All calculations are performed with the CP2K/Quickstep package [13,14]. The SCF optimizations are completed at the DFT level of theory, using the GGA functional Perdew–Burke–Ernzerhof (PBE) [15]. The double-zeta quality basis set DZVP-MOLOPT-SR-GTH, optimized for the properties of gas and condensed phase systems, is applied to all atoms [16]. The electronic wavefunction is expanded in the Gaussian Plane Wave (GPW) method [17,18]. Only valence electrons are modeled explicitly. The core electronic shells are represented as Goedecker–Teter–Hutter (GTH) pseudopotentials, optimized for PBE [19,20]. The charge density cutoff of the finest grid level is 400 Ry. Dispersion interactions are accounted for in all calculations. The latest D3 revision of the DFT + D method is used with the enabled three-body term [21].

When appropriate, periodic boundary conditions (PBC) are used. All systems are optimized in terms of the atomic coordinates and cell dimensions (if applicable) using the Broyden–Fletcher–Goldfarb–Shanno (BFGS) algorithm [22–25]. All property calculations are carried out over optimized structures.

3. Results

3.1. Basic Analysis of Adsorption

The corrugation of the graphene layer prohibits hexagonal symmetry. All adsorbate/G/SiC systems have space group P1. In our previous research, we discovered that a staggered orientation between the aromatic rings of the ligands and graphene rings is optimal for the adsorbance of π-electrons [10]. This principle is applied in the pre-optimized geometries of the PhH and TCDD complexes. However, staggered orientation is not applicable in the case of diazepam due to its low symmetry. The PhH and TCDD systems remain in the staggered intermolecular configuration at the end of the optimization.

The optimized geometry of D/G/SiC is shown in Figure 1.

As evident in our previous research, the employed methods yield the typical structure of pristine graphene after cell optimization [26]. Adsorption causes stabilization due to partially negating unbalanced surface forces in the involved species. One effect of this process is the geometrical alteration of the structures. The adsorption of discrete organic molecules applies a non-homogenous electromagnetic field over the surface of the adsorbent. As a result, the surface bends around the ligand's location. This bending has been measured with three-point angles Ang_1 and Ang_2 (Figure 2). Significant changes within diazepam's structure are measured with torsions $Tors_1$ and $Tors_2$ (Figure 2).

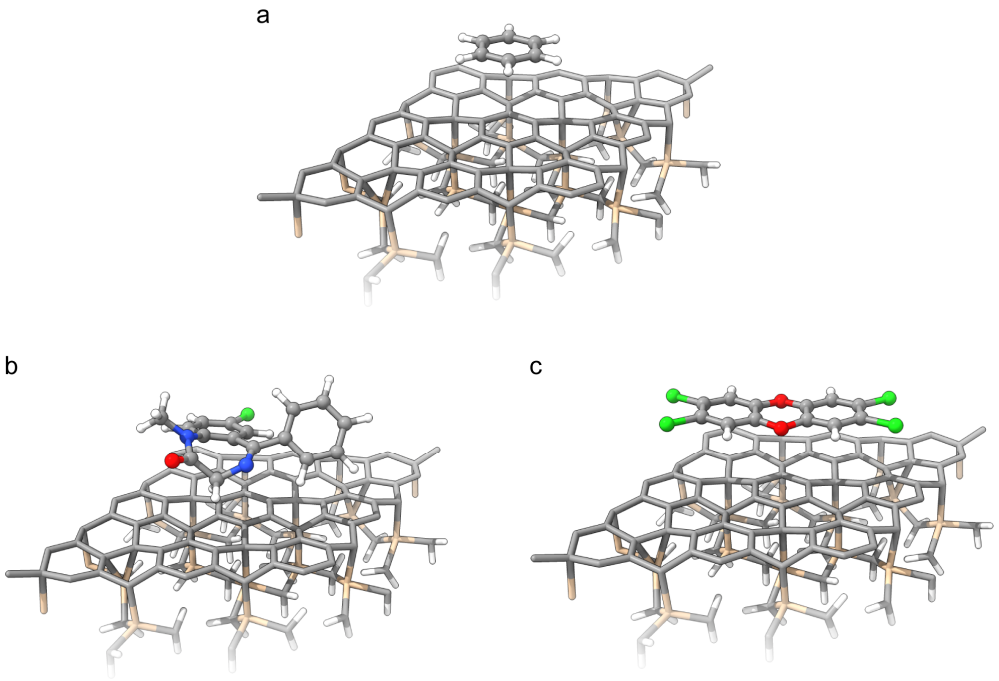

Figure 1. Optimized geometries of single cells of (**a**) PhH/G/SiC, (**b**) D/G/SiC and (**c**) TCDD/G/SiC. Although it may appear that there are tangled bonds, in the periodic supercells, all atoms exhibit the maximum valence. The gray balls denote the carbon atoms, and the gray sticks the bonds between them, while the red, blue and green balls denote the oxygen, nitrogen and chlorine atoms, respectively.

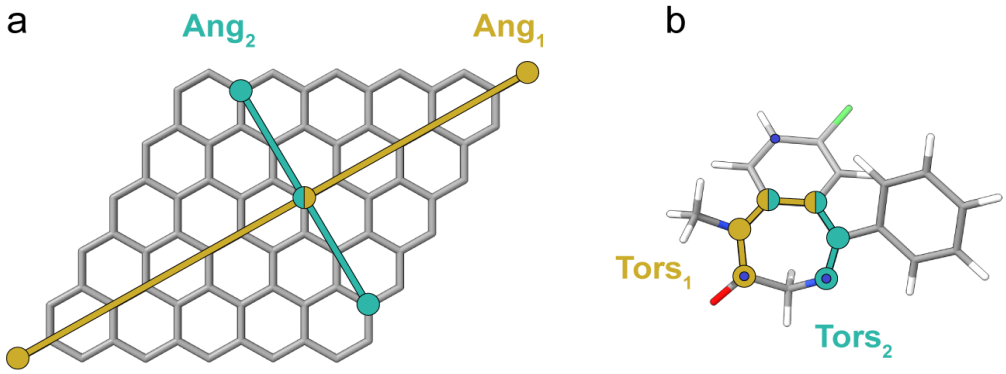

Figure 2. Significant 3- and 4-point angles in the geometry of (**a**) graphene and (**b**) diazepam. Note the atoms, designated with blue dots in (**b**)—their nuclei define the reference plane for the density plots.

PhH has a single, 6-electron π-system and, accordingly, its adsorption has the lowest energetic effect (E_{stab}) among the studied processes. However, due to the size of benzene, more molecules of its kind can be adsorbed per unit surface area compared to D or TCDD.

The geometry of D is far from planar and, in fact, the molecule belongs to point group C1. The shortest ($Dist_{least}$) and the average distances ($Dist_{mean}$) between this ligand and the corrugated G are the largest among those studied (Table 1). Still, diazepam contains 5 lone pairs (LP) and 18 π-electrons in 2 (12- and 6-electron) conjugated, aromatic systems. Most of its n- and π-density is oriented favorably for stacking with the π-MOs of the corrugated graphene. Hence, E_{stab}(D/G/SiC) is more than twice E_{stab}(PhH/G/SiC). Surprisingly, the bending of the corrugated graphene sheet (Ang_1 and Ang_2 in Table 1) is slightly lower in the presence of D than in clean G/SiC. This result corresponds well with the high $Dist_{least}$ and $Dist_{mean}$ values. A possible explanation is as follows: not only does D have to assume a geometry closer to planar, but G also has to adjust, for the maximum benefit,

the intermolecular attraction. Two torsion angles are selected to measure the flattening of the ligand (Figure 2). Adsorption alters both $Tors_1$ and $Tors_2$ towards a more in-plane geometry in the 3H-1,4-benzodiazepine moiety. The dihedrals change by 4.17 and 13.19 deg., respectively.

Table 1. Geometrical and energetic data for the adsorbate/G/SiC systems (System): inter-ring orientation (Orient), graphene bending angle Ang_1 (Ang_1), graphene bending angle Ang_2 (Ang_2), shortest adsorbent–graphene distance ($Dist_{least}$), average adsorbent–graphene distance ($Dist_{mean}$) and energetic effect of adsorption (E_{stab}).

System	Orient	Ang_1	Ang_2	$Dist_{least}$	$Dist_{mean}$	E_{stab} [kJ/mol]
G/SiC		177.87	176.57	-	-	-
PhH/G/SiC	AB	177.79	176.39	3.39	3.46	42
D/G/SiC	-	178.08	176.88	3.49	3.91	88
TCDD/G/SiC	AB	177.79	176.37	3.28	3.43	114

With a half-life of 5.8–11.3 years in humans [27], the toxicity of TCDD manifests through mechanisms that are entirely based on intermolecular attraction. Additionally, the pi-electronic system of this carcinogen is much larger than that of PhH. Moreover, as opposed to D, dioxin has an entirely planar geometry, arranged in hexagons, which enables optimal π-π stacking with graphene. Unsurprisingly, TCDD exhibits the highest theoretical absorption potential among the studied candidates and by all factors (Table 1).

PBE + D3 is known for the accurate prediction of the binding energies of systems with weak interactions [28] (mean absolute deviation: 2.09 kJ/mol).

3.2. Chemosensor Properties

When both the adsorbent and adsorbate have a band gap, the proximity of the frontier orbitals may result in a two-way response between the participating systems, indicated by clear alterations in the HOMO–LUMO region of the band structure (BS) (Figure 3) and the projected density of states (PDOS) (Figure 4). While the absolute energy levels of the G/SiC frontier MOs remain approximately the same after each adsorption, the corresponding values for the ligands change significantly (Table 2). The BS of pure A- the clean G/SiC substrate and the adsorbent/G/SiC complex are illustrated, in this order, for PhH, TCDD and D in Figures 3, 5 and 6, respectively. The corresponding PDOS results, in the same ligand order, are given in Figures 4, 7 and 8. All energy levels in the aforementioned figures and in Table 2 are relative to the HOMO of the G/SiC system, so this reference orbital is located at 0.00 eV. The BS figures of the pure adsorbates can be regarded as simple MO energy diagrams and are only included to enable the visual comparison of the electronic structures before and after adsorption. Figures 3, 5 and 6 display the absolute shifts in energy for both the adsorbate's and the adsorbent's frontier MOs due to complex formation. One can also find the relative positions of the ligand's HOMO and LUMO orbitals among the G/SiC MOs after adsorption. As expected, once the ligands bind to the crystalline system, k-point anisotropy becomes evident in their frontier MOs. White adsorption alters the band gaps of PhH and TCDD by only 0.01 eV (Figures 3 and 5), while the HOMO–LUMO difference for D decreases by 0.21 eV, from 3.03 to 2.82 eV (Figure 6). Such a change is entirely sufficient for chemosensor activity. As expected, the larger geometrical and band gap changes in the case of diazepam are accompanied by larger anisotropy in the k-point energy levels of the frontier MOs.

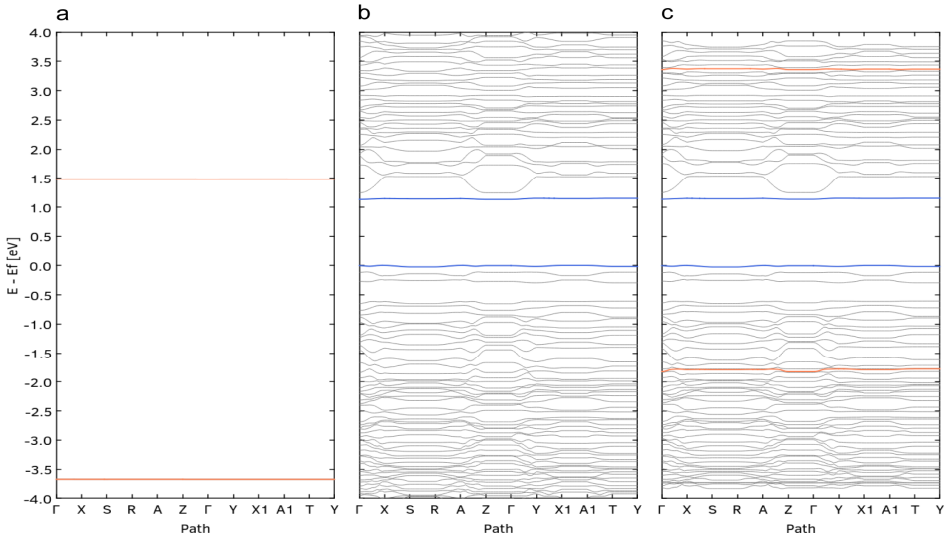

Figure 3. Band structures of (**a**) PhH, (**b**) G/SiC and (**c**) PhH/G/SiC. The frontier orbitals are colored in blue for G/SiC and orange for PhH. The values of all diagrams are adjusted to the same scale, in which the HOMO of the clean G/SiC is at 0 eV.

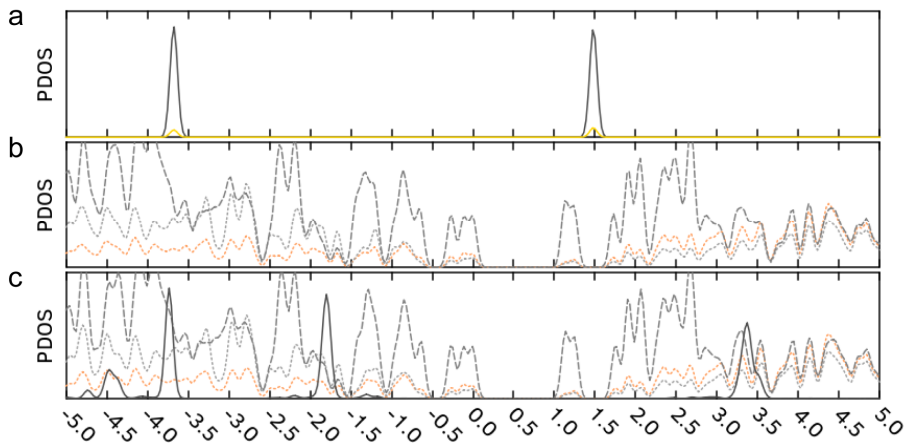

Figure 4. PDOS of (**a**) the adsorbent, (**b**) the adsorbate and (**c**) the adsorbent–adsorbate system PhH/G/SiC. Dotted lines are for the C and Si atoms in SiC. Dashed lines are for the C atoms of graphene. Continuous lines are for the H and C atoms in PhH. Si is in orange, C is in gray and H is in gold. The values of all diagrams are adjusted to the same scale, in which the HOMO of the clean G/SiC is at 0 eV.

Table 2. Orbital energies and their differences for adsorbents, clean G/SiC (A) and the adsorbent/G/SiC (Ads) systems: HOMO of the lone adsorbate (HOMO), LUMO of the lone adsorbate (LUMO), band gap of the lone adsorbate (E_g), G/SiC HOMO after adsorption ($HOMO_s$), G/SiC LUMO after adsorption ($LUMO_s$), G/SiC band gap after adsorption (E_{gs}), adsorbate HOMO after adsorption ($HOMO_a$), adsorbate LUMO after adsorption ($LUMO_a$) and band gap after adsorption (E_{ga}). All values are in eV. All values are according to BS diagrams. All BS diagrams were adjusted, so the HOMO of the clean G/SiC is at 0 eV [A]. Values for clean G/SiC.

Ads	HOMO	LUMO	E_g	$HOMO_s$	$LUMO_s$	E_{gs}	$HOMO_a$	$LUMO_a$	E_{ga}
[A]	0.00	1.14	1.14	-	-	-	-	-	-
PhH	−3.67	1.48	5.15	0.00	1.14	1.14	−1.79	3.37	5.16
D	−1.60	1.43	3.03	0.00	1.13	1.13	−1.08	1.74	2.82
TCDD	−1.80	1.43	3.23	0.00	1.12	1.12	−0.78	2.44	3.22

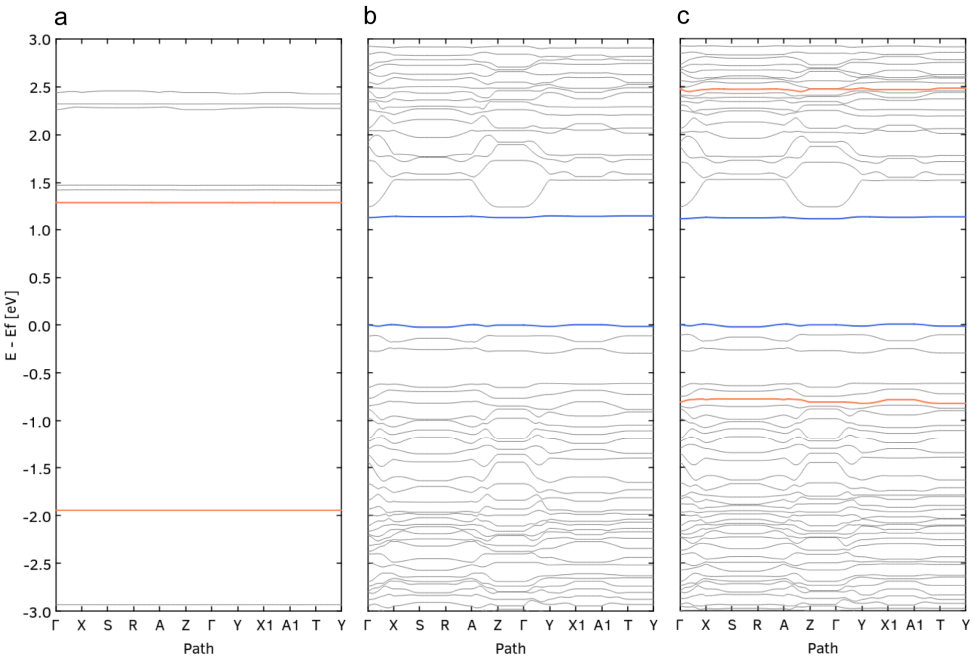

Figure 5. Band structures of (**a**) TCDD, (**b**) G/SiC and (**c**) TCDD/G/SiC. The frontier orbitals are colored in blue for G/SiC and orange for TCDD. The values of all diagrams are adjusted to the same scale, in which the HOMO of the clean G/SiC is at 0 eV.

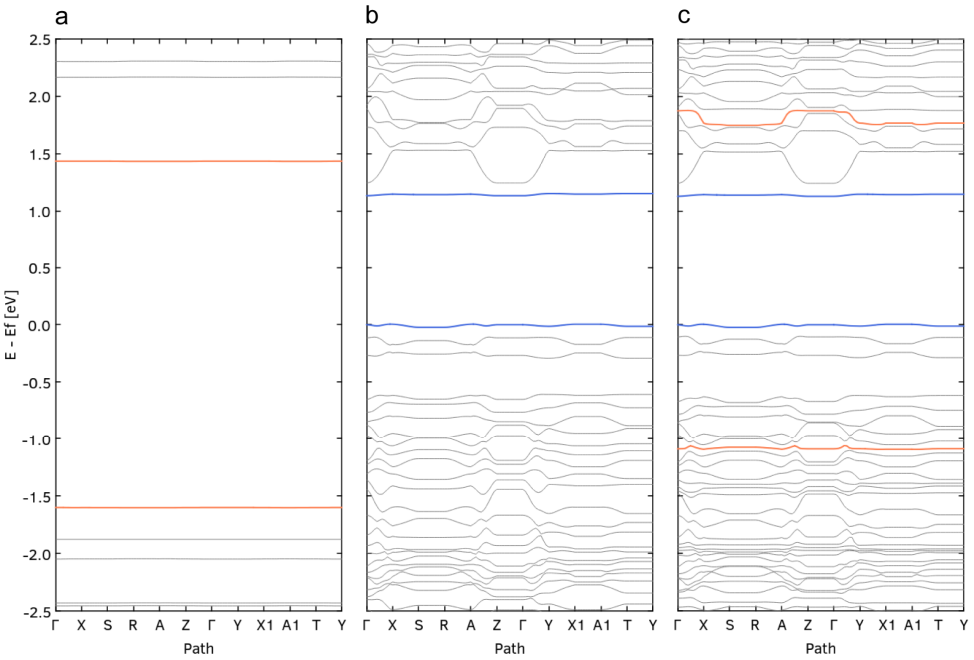

Figure 6. Band structures of (**a**) D, (**b**) G/SiC and (**c**) D/G/SiC. The frontier orbitals are colored in blue for G/SiC and orange for D. The values of all diagrams are adjusted to the same scale, in which the HOMO of the clean G/SiC is at 0 eV.

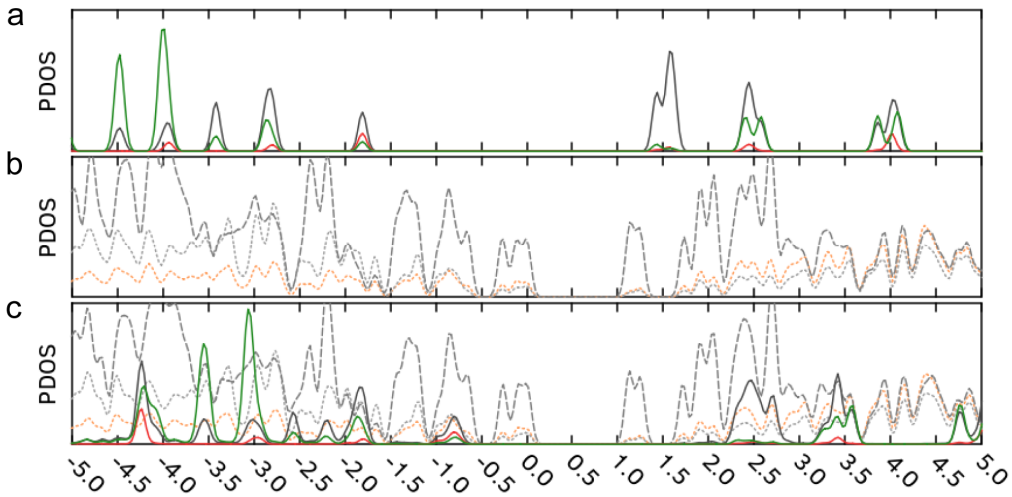

Figure 7. PDOS of (**a**) the adsorbent, (**b**) the adsorbate and (**c**) the adsorbent–adsorbate system TCDD/G/SiC. Dotted lines are for the C and Si atoms in SiC. Dashed lines are for the C atoms of graphene. Continuous lines are for the H, C, O and Cl atoms in TCDD. Si is in orange, C is in gray, H is in dark yellow, O is in red and Cl is in green. The values of all diagrams are adjusted to the same scale, in which the HOMO of the clean G/SiC is at 0 eV.

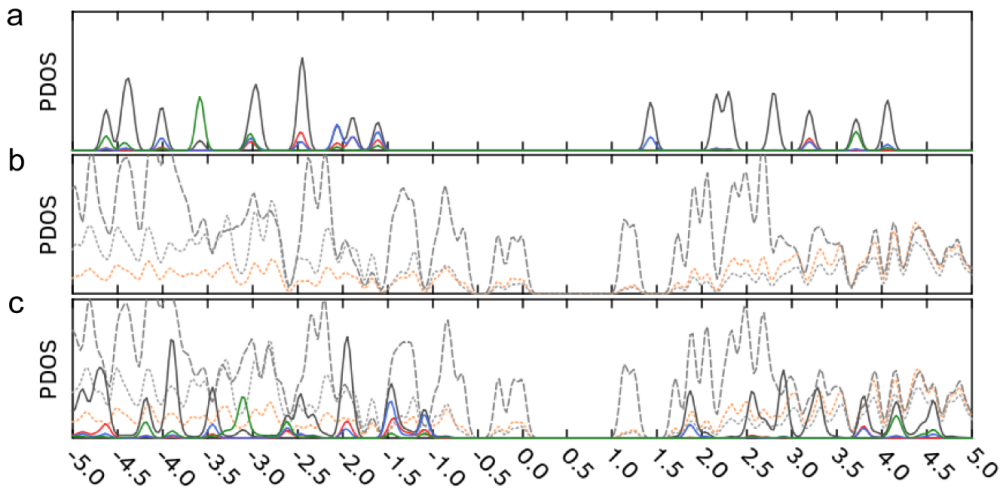

Figure 8. PDOS of (**a**) the adsorbent, (**b**) the adsorbate and (**c**) the adsorbent–adsorbate system D/G/SiC. Dotted lines are for the C and Si atoms in SiC. Dashed lines are for the C atoms of graphene. Continuous lines are for the H, C, N, O and Cl atoms in D. Si is in orange, C is in gray, N is in blue, O is in red and Cl is in green. The values of all diagrams are adjusted to the same scale, in which the HOMO of the clean G/SiC is at 0 eV.

Modeling the molecular structures with the same combination of method and basis set guarantees that the deviations will be mostly systematic. In other words, the size property shift is, by approximation, the same for each similar system. Therefore, estimating the changes in the band gaps (by subtraction) negates the systematic component of the said deviation and results in errors, being well below the mean absolute deviation (MAD) for the method. The MAD in predicting the electronic properties for PBE is between 0.09 and 0.16 eV [29]. The MAD of the method is below the value of the change in the band gap for non-planar systems with π-conjugation.

Adsorption causes noticeable changes in the state density profiles of all participants in the examined systems. Various peaks are altered in terms of width, height and element contribution. Occasionally, there are even qualitative changes in the topology of zones with adjacent peaks.

The robustness of graphene can explain the minimal changes in the electronic structure of the adsorbent. Chemically, defectless G is considered extremely inert [30]. Due to its tensile strength (130 GPa) [31] and Young's modulus (~1 TPa) [31], this carbon allotrope is known as "the strongest material ever tested". The entire π-density of this allotrope exists in the form of a planar, conjugated, aromatic system—the most stable π-electronic formation possible. Covalent bonding to SiC further prohibits structural changes in graphene.

PhH and TCDD are completely planar molecules and adsorption over a flat material does not explain the changes in their geometry and hence their energetics. While the absolute values of the energy levels of the frontier orbitals of PhH and TCDD change due to adsorption, the changes in the band gap are, as already mentioned, negligible. The 3H-1,4-benzodiazepine moiety in diazepam, on the other hand, has to assume a more planar form for a more efficient intermolecular interaction with the corrugated graphene. The band gap of the adsorbate decreases due to better conjugation, caused by the flatter atomic skeleton of the π-density. The electronic density stacking between the drug and the heterostructure is favorable enough to not only cover the energy difference for the geometrical changes in the ligand but also to result in binding potential energy of 88.62 kJ/mol. This value is comparable with the reaction barriers in organic chemistry. Apparently, the G/SiC substrate can be used as an active material in selective chemosensors for the detection/indication of molecules with out-of-plane π-electronic density.

The intermolecular interaction in the D/G/SiC complex introduces anisotropy within the energy levels of the frontier orbitals of D with respect to different k-points. A comparison of Figure 6a,c demonstrates this result. On the other hand, the field of the ligand induces almost no changes in the BS of the adsorbent (Figure 6b vs. Figure 6c).

4. Conclusions

We investigated the potential of semiconducting, corrugated graphene, grown on silicon carbide, as an active element in chemosensors. For this purpose, we modeled the adsorption of benzene, diazepam and 2,3,7,8-tetrachlorodibenzo-*p*-dioxin on the material's surface. The energetic effects of the intermolecular processes were 42, 88 and 114 kJ/mol, respectively. According to the graphene sheet bending and adsorbate–adsorbent distances, the heterostructure favors the ligands in the following order: diazepam < benzene < TCDD. The apparent ambiguity in the results for diazepam is easy to explain. The abundance of lone pairs and π-electrons compensates for the low-symmetry, non-planar, far from optimal (adsorption-wise) geometry. In fact, the binding energy is comparable with the reaction barriers in organic chemistry.

The maximum band gap change in the heterostructure, caused by adsorption, is 0.02 eV. This result corresponds to the relative chemical and physical inertness of graphene and its geometrical stiffness, further augmented by the SiC substrate. Intermolecular binding does not alter the HOMO–LUMO difference in benzene and TCDD by more than 0.01 eV. These completely planar molecules were not expected to undergo significant geometrical changes; hence, the alterations in their frontier orbitals were also minimal.

The adsorption of diazepam caused significant changes in the PDOS of both structures in the complex. The peaks were altered in terms of the relative position, width, height and element contribution. There were qualitative changes in the topology of zones with adjacent peaks. This ligand underwent the significant contraction of its band gap, namely by 0.21 eV. This value is more than sufficient to prove the efficiency of corrugated graphene as a selective chemosensor. The very disadvantages of the ligand's geometry are advantageous for its chemodetection.

In conclusion, corrugated graphene is applicable as an active material in selective chemosensors for non-planar aromatic molecules.

Author Contributions: Conceptualization, T.M. and S.K.; methodology, D.A.K., T.M., S.K. and D.T.; software, D.A.K., S.K. and D.T.; validation, T.M., S.K. and I.A.; formal analysis, D.A.K., S.K. and D.T.; investigation, D.A.K., S.K., P.I., D.D. and I.A.; resources, T.M.; data curation, T.M.; writing—original draft preparation, D.A.K., S.K. and T.M.; writing—review and editing, T.M., D.D., P.I. and I.A.;

visualization, D.A.K. and D.T.; supervision, T.M. and I.A.; project administration, T.M.; funding acquisition, T.M. All authors have read and agreed to the published version of the manuscript.

Funding: This research was supported financially by the National Science Fund of Bulgaria under grant KP-06-H58/2-16.11.2021.

Institutional Review Board Statement: Not applicable.

Informed Consent Statement: Not applicable.

Data Availability Statement: Data is contained within the article.

Acknowledgments: The numerical calculations were partially carried out on the high-performance computing system AVITOHOL at the Institute of Information and Communication Technologies, Bulgarian Academy of Sciences.

Conflicts of Interest: The authors declare no conflicts of interest.

References

1. Li, X.; Cai, W.; An, J.; Kim, S.; Nah, J.; Yang, D.; Piner, R.; Velamakanni, A.; Jung, I.; Tutuc, E.; et al. Large-Area Synthesis of High-Quality and Uniform Graphene Films on Copper Foils. *Science* **2009**, *324*, 1312–1314. [CrossRef]
2. Reina, A.; Jia, X.; Ho, J.; Nezich, D.; Son, H.; Bulovic, V.; Dresselhaus, M.; Kong, J. Large area, few-layer graphene films on arbitrary substrates by chemical vapor deposition. *Nano Lett.* **2009**, *9*, 30. [CrossRef] [PubMed]
3. Huang, L.; Chang, Q.; Guo, G.; Liu, Y.; Xie, Y.; Wang, T.; Ling, B.; Yang, H. Synthesis of high-quality graphene films on nickel foils by rapid thermal chemical vapor deposition. *Carbon* **2012**, *50*, 551. [CrossRef]
4. Park, J.; Xiong, W.; Gao, Y.; Qian, M.; Xie, Z.; Mitchell, M.; Zhou, Y.; Han, G.; Jiang, L.; Lu, Y. Fast growth of graphene patterns by laser direct writing. *Appl. Phys. Lett.* **2011**, *98*, 123109. [CrossRef]
5. Berger, C.; Song, Z.; Li, T.; Li, X.; Ogbazghi, A.; Feng, R.; Dai, Z.; Marchenko, A.; Conrad, E.; First, P.; et al. Ultrathin Epitaxial Graphite: 2D Electron Gas Properties and a Route toward Graphene-based Nanoelectronics. *J. Phys. Chem.* **2004**, *108*, 19912. [CrossRef]
6. Nevius, M.; Conrad, M.; Wang, F.; Celis, A.; Nair, M.; Taleb-Ibrahimi, A.; Tejeda, A.; Conrad, E. Semiconducting Graphene from Highly Ordered Substrate Interactions. *Phys. Rev. Lett.* **2015**, *115*, 136802. [CrossRef] [PubMed]
7. Berger, C.; Conrad, E.H.; de Heer, W.A. *Numerical Data and Functional Relationships in Science and Technology—New Series*; Subvolume III/45B; Springer: Berlin/Heidelberg, Germany, 2017. [CrossRef]
8. Kolev, S.; Atanasov, V.; Aleksandrov, H.; Milenov, T. Band gap modulation of graphene on SiC. *Eur. Phys. J. B* **2018**, *91*, 272. [CrossRef]
9. Kolev, S.; Atanasov, V.; Aleksandrov, H.; Popov, V.; Milenov, T. Semiconducting graphene. *Bul. Chem. Commun.* **2019**, *51*, 552–556. [CrossRef]
10. Kolev, S.K.; Aleksandrov, H.A.; Atanasov, V.A.; Popov, V.N.; Milenov, T.I. Interaction of Graphene with Out-of-Plane Aromatic Hydrocarbons. *J. Phys. Chem. C* **2019**, *123*, 21448–21456. [CrossRef]
11. MSDS of Benzene. Available online: https://www.airgas.com/msds/001062.pdf (accessed on 26 September 2024).
12. MSDS of TCDD. Available online: https://www.bio.vu.nl/~microb/Protocols/chemicals/MSDS/tetrachlorodibenzo-p-dioxin%20(2,3,7,8-).pdf (accessed on 26 September 2024).
13. VandeVondele, J.; Krack, M.; Mohamed, F.; Parrinello, M.; Chassaing, T.; Hutter, J. Quickstep: Fast and accurate density functional calculations using a mixed Gaussian and plane waves approach. *Comput. Phys. Commun.* **2005**, *167*, 103–128. [CrossRef]
14. Kuehne, T.D.; Iannuzzi, M.; Del Ben, M.; Rybkin, V.V.; Seewald, P.; Stein, F.; Laino, T.; Khaliullin, R.Z.; Schuett, O.; Schiffmann, F.; et al. CP2K: An electronic structure and molecular dynamics software package—Quickstep: Efficient and accurate electronic structure calculations. *J. Chem. Phys.* **2020**, *152*, 194103. [CrossRef]
15. Perdew, J.P.; Burke, K.; Ernzerhof, M. Generalized Gradient Approximation Made Simple. *Phys. Rev. Lett.* **1996**, *77*, 3865–3868. [CrossRef] [PubMed]
16. VandeVondele, J.; Hutter, J. Gaussian basis sets for accurate calculations on molecular systems in gas and condensed phases. *J. Chem. Phys.* **2007**, *127*, 114105. [CrossRef] [PubMed]
17. Lippert, G.; Hutter, J.; Parrinello, M. The Gaussian and augmented-plane-wave density functional method for ab initio molecular dynamics simulations. *Theor. Chem. Acc.* **1999**, *103*, 124–140. [CrossRef]
18. Lippert, G.; Hutter, J.; Parrinello, M. A hybrid Gaussian and plane wave density functional scheme. *Mol. Phys.* **1997**, *92*, 477–487. [CrossRef]
19. Goedecker, S.; Teter, M.; Hutter, J. Separable dual-space Gaussian pseudopotentials. *Phys. Rev. B* **1996**, *54*, 1703–1710. [CrossRef]
20. Hartwigsen, C.; Goedecker, S.; Hutter, J. Relativistic separable dual-space Gaussian pseudopotentials from H to Rn. *Phys. Rev. B* **1998**, *58*, 3641–3662. [CrossRef]
21. Grimme, S.; Antony, J.; Ehrlich, S.; Krieg, H. A consistent and accurate ab initio parametrization of density functional dispersion correction (DFT-D) for the 94 elements H-Pu. *J. Chem. Phys.* **2010**, *132*, 154104. [CrossRef]
22. Broyden, C. The convergence of a class of double-rank minimization algorithms. *J. Inst. Math. Appl.* **1970**, *6*, 76–90. [CrossRef]

23. Fletcher, R. A new approach to variable metric algorithms. *Comp. J.* **1970**, *13*, 317–322. [CrossRef]
24. Goldfarb, D. A family of variable-metric methods derived by variational means. *Math. Comp.* **1970**, *24*, 23–26. [CrossRef]
25. Shanno, D. Conditioning of quasi-Newton methods for function minimization. *Math. Comp.* **1970**, *24*, 647–656. [CrossRef]
26. Kolev, S.; Balchev, I.; Cvetkov, K.; Tinchev, S.; Milenov, T. Ab-Initio molecular dynamics simulation of graphene sheet. *J. Phys. Conf. Ser.* **2017**, *780*, 012014. [CrossRef]
27. Olson, J.R. Pharmacokinetics of Dioxins and Related Chemicals. In *Dioxins and Health*; Schecter, A., Ed.; Springer: Boston, MA, USA, 1994; pp. 154–196.
28. Grimme, S.; Hansen, A.; Brandenburg, J.G.; Bannwarth, C. Dispersion-Corrected Mean-Field Electronic Structure Methods. *Chem. Rev.* **2016**, *116*, 5105–5154. [CrossRef]
29. Xu, X.; Goddard, W.A. The extended Perdew-Burke-Ernzerhof functional with improved accuracy for thermodynamic and electronic properties of molecular systems. *J. Chem. Phys.* **2004**, *121*, 4068–4082. [CrossRef]
30. Liao, L.; Peng, H.; Liu, Z. Chemistry Makes Graphene beyond Graphene. *J. Am. Chem. Soc.* **2014**, *136*, 12194–12200. [CrossRef]
31. Lee, C.; Wei, X.; Kysar, J.W.; Hone, J. Measurement of the Elastic Properties and Intrinsic Strength of Monolayer Graphene. *Science* **2008**, *321*, 385–388. [CrossRef]